

PCCP

Accepted Manuscript



This is an *Accepted Manuscript*, which has been through the Royal Society of Chemistry peer review process and has been accepted for publication.

Accepted Manuscripts are published online shortly after acceptance, before technical editing, formatting and proof reading. Using this free service, authors can make their results available to the community, in citable form, before we publish the edited article. We will replace this *Accepted Manuscript* with the edited and formatted *Advance Article* as soon as it is available.

You can find more information about *Accepted Manuscripts* in the [Information for Authors](#).

Please note that technical editing may introduce minor changes to the text and/or graphics, which may alter content. The journal's standard [Terms & Conditions](#) and the [Ethical guidelines](#) still apply. In no event shall the Royal Society of Chemistry be held responsible for any errors or omissions in this *Accepted Manuscript* or any consequences arising from the use of any information it contains.

Ligand Influence on the Electronic Spectra of Monocationic Copper-Bipyridine Complexes

Shuang Xu¹, Samer Gozem,² Anna I. Krylov,² Casey R. Christopher³ and J. Mathias Weber^{3*}

¹*JILA and Department of Physics, University of Colorado, Boulder, CO 80309-0440, USA*

²*Department of Chemistry, University of Southern California,
Los Angeles, CA 90089-0482, USA*

³*JILA and Department of Chemistry and Biochemistry, University of Colorado,
Boulder, CO 80309-0440, USA*

Abstract

We show photodissociation spectroscopy and computational analysis of three monocationic Cu-bipyridine complexes with one additional ligand of different interaction strength (N₂, H₂O and Cl) in the visible and UV. All three complexes show similar $\pi\pi^*$ bands with origins slightly above 4 eV and vibrational band contours that are due to bipyridine ring deformation modes. Experiments at low temperature show that excited-state lifetime is the limiting factor for the width of the vibrational features. In the case of Cl as a ligand, there is a lower lying bright ligand-to-ligand charge-transfer state around 2.75 eV. The assignment of the transitions was made based on equation-of-motion coupled-cluster calculations. While the nature of the ligand does not significantly change the position of the bright $\pi\pi^*$ state, it drastically changes the excited-state dynamics.

*Corresponding author; email: weberjm@jila.colorado.edu

I. Introduction

Copper complexes are important species in many areas of chemistry due to the abundance and low cost of copper and the availability of well-established syntheses for many types of copper-based metal organic complexes. For example, there is great hope that copper-based catalysts can replace some of the more expensive catalysts based on platinum group metals for water oxidation.¹ In photochemical and photophysical applications, Cu(I) complexes are particularly interesting, since the absence of low lying d-d excited states removes some of the most important radiationless de-excitation pathways, affording longer excited-state lifetimes and fluorescence applications.²

In metal-organic chemistry, imine-type ligands constitute one of the most important ligand classes, and bipyridine ligands are particularly interesting due to their relative simplicity and their ability to interact with many different metals.

The photophysics of bipyridine has received much attention in the past 30 years.³⁻¹⁰ In the present work, we exclusively use 2,2'-bipyridine (bipy) and we will restrict our discussion to this isomer. The lowest excited states of bipy are in the UV spectral region. Since bipy is of C_{2v} symmetry, only transitions to A_1 , B_1 and B_2 states are optically allowed. Transitions from the ground state to the S_1 (1^1A_2 , $n\pi^*$) state are symmetry forbidden, while the S_2 (1^1B_1 , $n\pi^*$) state is only weakly optically accessible, and the first bright transition is to the S_3 (1^1B_2 , $\pi\pi^*$) state. Notably, some of the character of the electronic transitions of bipy is preserved in complexes with transition metals.

Copper(I) polypyridyl complexes have been widely studied, such as homoleptic $Cu^I(pp)_2$ (pp = polypyridyl ligand, e. g., bipy or phenanthroline derivatives).¹¹⁻¹⁷ In solution, the photophysics of such systems sensitively depends on the solvent.¹¹⁻¹⁴ A very powerful way of tuning the

photophysical and photochemical properties of such complexes lies in using different substituents on the organic ligands. In copper(I) complexes with more than one pp ligand, strong metal-to-ligand charge-transfer (MLCT) bands are usually observed. Similar to other transition metal complexes, this opens possible applications in solar energy conversion.¹⁸⁻²⁵

In contrast to the more widely studied copper(I) complexes with more than one pp ligand, systems with only one pp ligand have not been thoroughly investigated. In solution, the complexity brought about by speciation can make the study of the intrinsic photophysics of molecular species difficult. Additionally, solvation effects generally broaden the spectroscopic response of the molecule under study. Spectroscopy of mass selected ions *in vacuo* circumvents these difficulties and allows investigation of the electronic structure of molecular ions in greater detail than possible in condensed phase experiments. This also makes it easier to benchmark quantum chemical calculations without worrying about solvent effects.

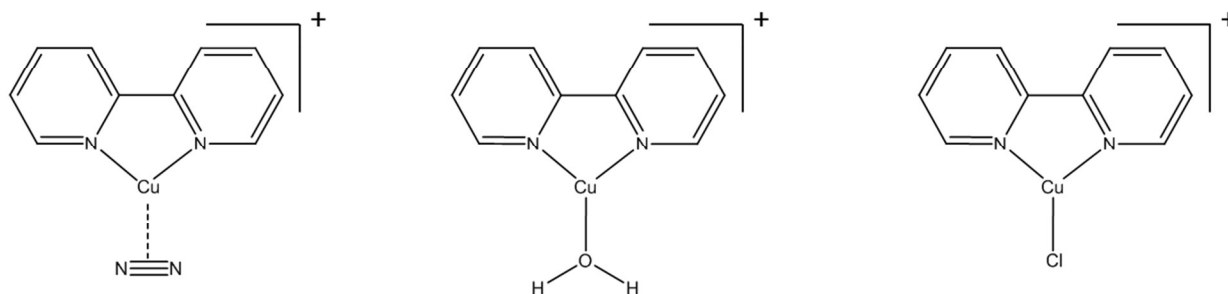


Figure 1. Copper complexes under study in this work. The complexes with $L = \text{N}_2$ and H_2O (left and center) have singlet ground states, while the ground state of the complex with $L = \text{Cl}$ (right) is a doublet.

In the present work, our focus lies on the photophysics of heteroleptic monocationic copper complexes with one bipy and one additional ligand (see Figure 1; for simplicity, we abbreviate (bipy)Cu as **Cu**). In this joint experimental and computational work, we present electronic spectra of complexes of the form $[\text{Cu-L}]^+$ with $L = \text{N}_2$, H_2O and Cl , representing very different

unit (inset shows details); H: ion lens and deflectors; I: mass gate; J: reflectron; K: microchannel plate detector; L: laser power meter.

Ions are generated under ambient conditions by ESI. After desolvation in a heated stainless-steel capillary, ions enter the first differential pumping stage, where they are focused with a short tube lens into a skimmer. Next, the ions travel in a series of three octupole ion guides through three differential pumping regions. The ions are then deflected by a quadrupole bender and injected into a Paul trap after passing through a short octupole guide, an Einzel lens and an additional tube lens at the entrance of the trap. The ions are accumulated in the trap and are cooled by collisions with buffer gas. The trap is mounted on the cold head of a closed cycle He cryostat and enclosed in a heat shield held at 60 K. After accumulation and cooling in the trap, the ions are injected into the acceleration region of a Wiley-McLaren time-of-flight mass spectrometer (TOF-MS).

In the first space focus of the TOF-MS, the ions of interest are mass selected by a pulsed mass gate and irradiated by a laser pulse shortly behind the mass gate. The light source used for the present work is an optical parametric oscillator (GWU PreciScan) pumped by the third harmonic of a Nd:YAG laser (Innolas Spitlight 600). The signal wave is tunable from 1.75 eV to 3.0 eV and has a 5 ns pulse duration and a 5 cm^{-1} bandwidth. Second harmonic generation and sum frequency mixing of the signal wave with 1064 nm radiation from the pump laser can be used to produce UV radiation up to 5.6 eV photon energy (GWU UV Scan). The complete spectral coverage is composed of several narrower, overlapping tuning ranges corresponding to different sets of nonlinear crystals.

If photofragments are formed after irradiation, they are separated from remaining parent ions by a two-stage reflectron and detected by a microchannel plate (MCP) detector. We monitor the yield of photofragments as a function of photon energy to record photodissociation spectra.

Typically, ca. 10-20 spectra are acquired in each spectral region and on different days and averaged.

II.2. Computational

Ground-state dissociation thresholds, natural charges, and vibrational frequencies in this work were computed with density functional theory³⁵ (DFT) using the PBE0 functional³⁶ and def2-TZVP³⁷ basis sets for all atoms. These calculations were performed using the TURBOMOLE suite of programs.³⁸

To assign the peaks observed in the action spectra to specific transitions, we computed the excitation energies and the respective oscillator strengths for low-lying excited states of $[\text{Cu-N}_2]^+$, $[\text{Cu-OH}_2]^+$, and $[\text{Cu-Cl}]^+$. The ground-state structures were optimized at the DFT level of theory with the ω B97X-D functional³⁹ and cc-pVTZ basis set. All structures were found to have C_{2v} symmetry.

Excitation energies were computed at the equation-of-motion for excitation energies coupled-cluster approach with single and double excitations^{40, 41} (EOM-EE-CCSD). The π - π^* state in $[\text{Cu-Cl}]^+$, which suffers from a spin-incomplete set of configurations generated from a doublet reference,⁴² was instead computed using the spin-flip variant of EOM (i.e., EOM-SF-CCSD) starting from a quartet reference,^{43, 44} as in our previous study of substituted vinyl radicals.⁴⁵ In addition to vertical excitation energies, we also computed adiabatic excitation energies using excited-state geometries optimized with ω B97X-D with C_{2v} symmetry enforced (thus, actual adiabatic excitation energies might be lower than those computed with C_{2v} constraint). All excited-state calculations employ the cc-pVTZ basis set, and were computed with C_{2v} symmetry enforced. To further reduce the computational cost of the EOM calculations, Cholesky decomposition (using the CD threshold of 10^{-2}) was used. Core orbitals were frozen in correlated calculations (the 1s orbitals of N, C, and O atoms, the 1s, 2s, and 2p orbitals of Cl, and the 1s, 2s, 2p, 3s, and 3p orbitals of Cu).⁴⁶ EOM-CC and DFT calculations with the ω B97X-D functional were conducted using the Q-Chem electronic structure program.^{47, 48}

III. Results and discussion

III.1. Overview

Some of the ground-state electronic properties of the complexes under study are summarized in Table 1. As one would expect, the ligand binding energy increases strongly going from N₂ to H₂O to Cl. Note that [Cu-Cl]⁺ is a doublet, while the other two complexes have singlet closed shell ground states. The N₂ and H₂O ligands are roughly neutral, and the positive charge of the complex is distributed over the Cu atom and the bipy ligand. The Cl ligand carries substantial negative charge, increasing the positive charge on the copper center and the bipy ligand. One interesting question is how far the concept of formal charges carries here, and how they are to be interpreted. One may be tempted to formally view the Cl ligand as a Cl⁻ anion. However, the deviation of the calculated partial charge on the Cu atom from +1 has the same magnitude as for the other two complexes, and the charge on the metal atom is much closer to +1 than to +2, since the positive charge on the bipy ligand also shows a marked increase. For L = N₂ and H₂O, it may be reasonable to describe the ground state as a combination of Cu(I) and Cu(0), while a mixture of Cu(I) and Cu(II) may be more appropriate for L=Cl.

Table 1. Calculated ground-state properties of the complexes under study (PBE0/def2-TZVP). Dissociation threshold energies are for the loss of the “L” ligand from $[\text{Cu-L}]^+$, except for $^1\text{Cu}^+$ where the threshold energy is given for dissociation into Cu and bipy⁺. Partial charges were determined using natural population analysis.

species	dissociation threshold [eV]	charge on Cu / ligand / bipy
$^1\text{Cu}^+$	(4.30)	0.886 / - / 0.114
$^1[\text{Cu-N}_2]^+$	0.30	0.918 / -0.081 / 0.163
$^1[\text{Cu-OH}_2]^+$	1.06	0.846 / -0.055 / 0.099
$^2[\text{Cu-Cl}]^+$	2.56	1.174 / -0.512 / 0.338

Figure 3 shows the electronic photodissociation spectra of $[\text{Cu-L}]^+$ ($L = \text{N}_2, \text{H}_2\text{O}, \text{Cl}$) in the UV at 250 K trap temperature. All spectra show similar characteristics with a peak around 4 eV, followed by an extended band contour towards higher energies (see Table 2). While no transitions were observed at lower energies for $L = \text{N}_2$ and H_2O , the spectrum for $L = \text{Cl}$ shows another band in the visible (see Table 2 and Section III.4). Comparison of the spectrum of the complex with $L = \text{N}_2$ with the absorption spectrum of $(\text{bipy})\text{Zn}^{2+}$ shows that the two complexes have nearly identical electronic spectra.⁵ Based on the assignment for the Zn^{2+} complex,⁵ the bright UV excited state in the Cu complexes should be of $\pi\pi^*$ character and localized on the bipy moiety.

The computational description of the electronic spectra of $[\text{Cu-L}]^+$ complexes is very challenging. Initial attempts to model the electronic spectra of $[\text{Cu-L}]^+$ complexes failed. Exploratory calculations based on time-dependent density functional theory (TD-DFT) with a number of different functionals yielded inconsistent results and were often strongly shifted from

the experimentally observed energies (e.g., by more than 0.8 eV). We note that using the omega-tuned, range separated BNL functional^{49, 50} did not yield satisfactory results, in contrast to our previous success with a similar compound, Ir(PPY)₃.⁵¹ Coupled-cluster calculations using the CC2 model also failed, probably because of a multi-configurational character of the ground state, as evaluated by the D₁ diagnostic proposed by Janssen and Nielsen.⁵² Calculations at the EOM-EE-CCSD level of theory indicate that each species has one optically bright excitation in the UV at ca. 4.65 eV (see Table 2). These calculations give vertical excitation energies for this transition that are systematically higher than the experiment by about 0.6 eV. The calculations confirm the $\pi\pi^*$ nature of the bright excited state and also show lower-lying dark states. Overall, it is not clear why the discrepancy between the EOM-CCSD excitation energies and the experimental peaks is larger than the typical EOM-CCSD error bars of ~ 0.3 eV. One possible explanation is an insufficient basis set. For example, a much better agreement was reported recently for electronic states of CuF⁻ using EOM-CCSD methods with the aug-cc-pVTZ-PP and ECP (on copper) and aug-cc-pVTZ (all other atoms) basis sets.⁵³ Another possibility for the difference between experimental and computed energies is that vibronic interactions with lower dark states might be responsible for distorting the band contour and shifting the peak position to lower energies.

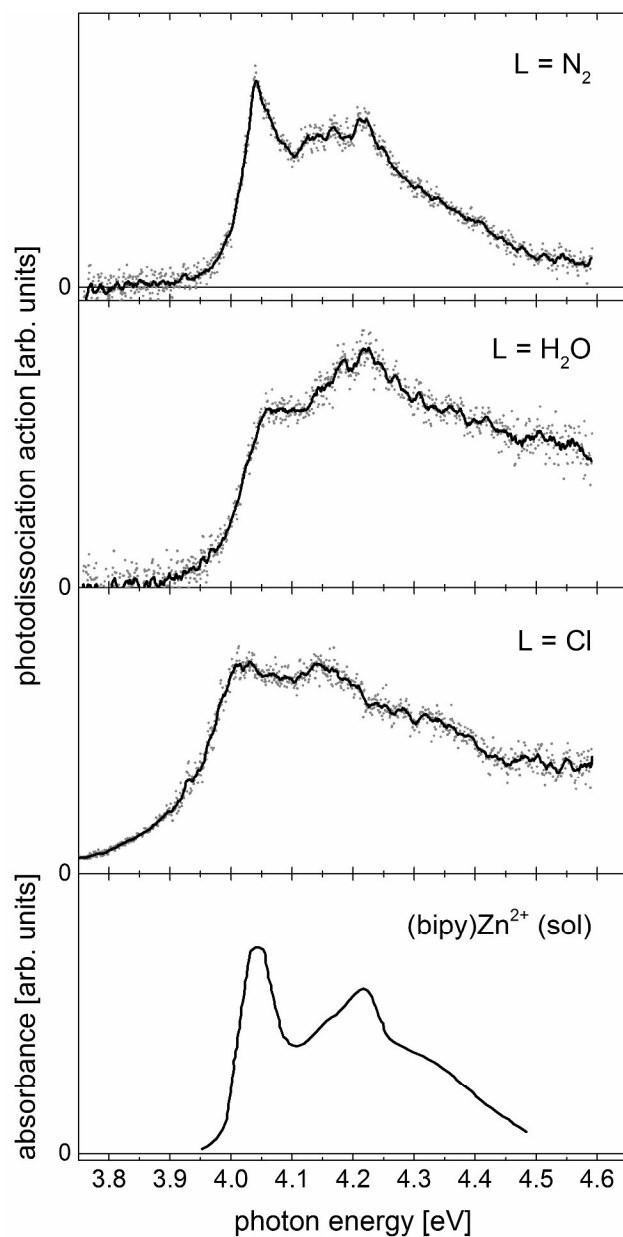


Figure 3. Electronic photodissociation spectra of $[\text{Cu-L}]^+$ complexes (top three panels) at 250 K and comparison with the absorption spectra of $(\text{bipy})\text{Zn}^{2+}$ (bottom panel) at 93 K in a water/methanol solution (digitized data taken from the work by Kotlicka *et al.*⁵). The points in the photodissociation spectra are the raw data, the full lines are the same data smoothed by 10-pt-adjacent averaging. The photodissociation signal corresponds to the loss of the ligand L in each case. Spectra of all three ions under study taken over the full range (2.1-4.5 eV) are also shown in Supplementary Information (Figure S2).

Table 2. Experimental and computed excitation energies. The experimental energies list the first discernible peaks in each electronic band. Computed energies are determined at the EOM-EE-CCSD/cc-pVTZ level unless indicated otherwise. Computed adiabatic excitation energies are in parentheses. All energies are given in eV.

species	experimental	calculated (adiabatic)	term	Oscillator strength	type
Cu^+	4.04				
$[\text{Cu-N}_2]^+$	– ^a	4.53	$^1\text{A}_2$	0	$\sigma\pi^*$
	4.04	4.65 (4.44)	$^1\text{B}_2$	0.047	$\pi\pi^*$
$[\text{Cu-OH}_2]^+$	– ^a	3.96	$^1\text{A}_2$	0	$\sigma\pi^*$
	– ^b	4.31	$^1\text{B}_2$	2.9×10^{-4}	MLCT to H_2O
	4.07	4.69 (4.62)	$^1\text{B}_2$	0.045	$\pi\pi^*$
$[\text{Cu-Cl}]^+$	– ^b	1.22	$^2\text{B}_2$	1.1×10^{-5}	
	– ^a	1.30	$^2\text{A}_2$	0	
	– ^b	1.84	$^2\text{B}_2$	2.2×10^{-4}	
	– ^b	1.87	$^2\text{B}_1$	2×10^{-6}	
	2.72	3.30 (2.54)	$^2\text{A}_1$	0.056	CT from Cl to bipy
	– ^b	3.48	$^2\text{B}_2$	2.4×10^{-5}	
	– ^a	3.53	$^2\text{A}_2$	0	
	4.02	4.62 (4.46) ^c	$^2\text{B}_2$	0.205 ^c	$\pi\pi^*$

^a This transition is symmetry-forbidden.

^b This band is allowed, but has negligible calculated oscillator strength, and is too weak to be observed experimentally.

^c These values were computed using EOM-SF-CCSD.

Excited-state optimization led to relatively small changes in the excited-state energies of the $\pi\pi^*$ state, slightly improving the agreement with experiment. The difference between the adiabatic and the experimental energy for the $\pi\pi^*$ state is 0.40 eV, 0.44 eV, and 0.55 eV for $[\text{Cu-N}_2]^+$, $[\text{Cu-Cl}]^+$, and $[\text{Cu-OH}_2]^+$, respectively.

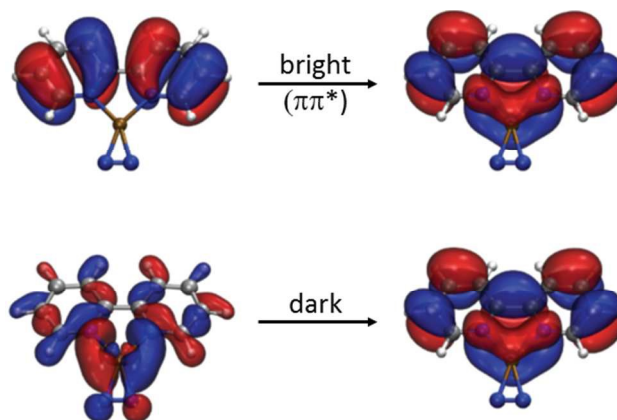


Figure 4. Leading molecular orbitals for the two lowest energy transitions in $[\text{Cu-N}_2]^+$. The upper panel shows the allowed transition to the $\pi\pi^*$ state, the lower panel shows the orbitals involved in the (symmetry forbidden) $\sigma\pi^*$ transition to the dark state calculated 0.12 eV below the bright $\pi\pi^*$ state (see also Table 2).

Our calculations at the EOM-EE-CCSD level of theory indicate that the bright states at ca. 4.0 eV for all complexes under study are of $\pi\pi^*$ character and that the transition orbitals are localized on the bipy moiety, as expected. In addition, all species have lower-lying dark states (see Table 2). In Cu^+ complexes, the dark states are of $\sigma\pi^*$ character instead of $n\pi^*$ (the latter being the case in isolated bipy), since the lower state orbitals strongly involve MOs that are chelating the Cu atom (see Figure 4), while these are essentially nonbonding in bare bipy. Comparison with the absorption spectrum of $(\text{bipy})\text{Zn}^{2+}$ in glassy solutions at low temperature suggests that the nature of the metal atom is not very relevant to the overall absorption spectrum,

provided that the metal ion is formally a closed shell species, which is true for both Cu^+ and Zn^{2+} .

In the following, we will discuss the spectra of all complexes in more detail and provide spectra at lower temperatures.

III.2. Weakly bound ligand – N_2

Figure 5 shows the photodissociation spectrum of $[\text{Cu-N}_2]^+$ at 70 K trap temperature. Lowering the temperature has a dramatic effect on the spectrum, and several sharper features can now be clearly resolved. We note that trap temperatures significantly below 70 K lead to condensing N_2 on the cold head and removing the parent ion from the mass spectrum. This indicates that – in contrast to the other two ligands – the $[\text{Cu-N}_2]^+$ complex formed in the trap rather than in the ESI source.

Since there is only one bright state calculated for each species, we assume that the observed substructure of the absorption band is due to vibrational progressions, controlled by Franck-Condon factors. Calculating Franck-Condon factors is very difficult given the problematic nature of the electronic structure calculations. However, we can identify candidates for Franck-Condon active vibrations by inspecting the ground-state vibrational modes of $[\text{Cu-N}_2]^+$ under the assumption that the energy differences of the vibrational modes in the ground and excited states are not too severe, similar to the approach taken in earlier studies of bipy.¹⁰ A geometry optimization of the $\pi\pi^*$ state in bipy (TDDFT with PBE0/def2-TZVP) reveals that the main geometry differences between bipy in the ground state and in the $\pi\pi^*$ state are the length of the central C-C bond and the CNC bond angle in the rings. For an allowed electronic transition, we

expect the totally symmetric vibrations to be the main contributors to the excited-state vibrational features.

The calculated energies of totally symmetric modes of $[\text{Cu-N}_2]^+$ that should be particularly active in these modes are represented in Figure 5 and compared to the experimental spectrum for $[\text{Cu-N}_2]^+$. The modes identified this way are mainly ring deformation modes, and they give a very good qualitative representation of the band contour. Bending and stretching modes of the CH groups, the N_2 stretch and the Cu- N_2 stretching mode should not be very Franck-Condon active and were therefore ignored for Figure 5. The calculated (ground state) and observed (excited state) peaks are collected in Table 3.

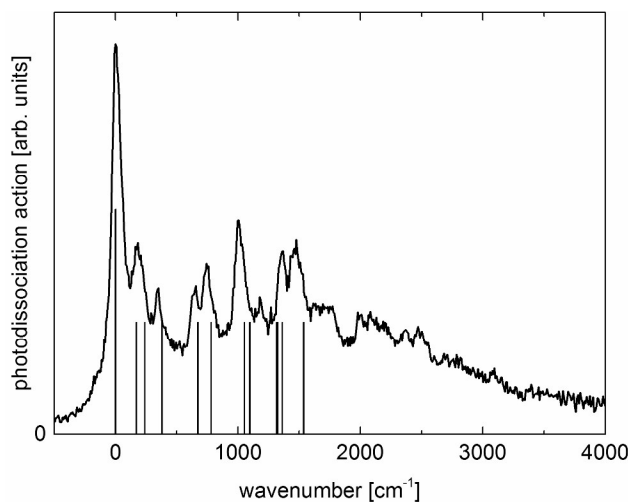


Figure 5. Photodissociation spectrum of $[\text{Cu-N}_2]^+$ at 70 K trap temperature. The wavenumber axis is relative to the 0-0 band position of the $\pi\pi^*$ electronic band, which is found at 4.04 eV. The full line represents experimental data, the stick spectrum shows calculated totally symmetric (ground state) vibrations of $[\text{Cu-N}_2]^+$ (see also Table 3). The 0-0 band is marked with a higher intensity for clarity, but we note that we cannot make any quantitative statements on the expected band intensities. The experiment monitored the loss of the N_2 ligand.

Table 3. Experimental values were determined by fitting Lorentzian profiles with 100 cm^{-1} full width at half-maximum (which corresponds to the width of the 0-0 band) to the clearly discernible peak features. The error in these peak positions is $\pm 10\text{ cm}^{-1}$. Calculated values are for totally symmetric ground-state vibrational modes of $[\text{Cu-N}_2]^+$ obtained with PBE0/def2-TZVP (harmonic approximation). Additional totally symmetric modes are listed in Supplementary Information, Table S1.

experimental [cm^{-1}]	calculated [cm^{-1}]	assignment
179 ^a	170/240	skeletal bipy bending modes
347	381	central C-C stretch
639	673	CNC bending ring deformation
747	783	CCC bending ring deformation
1004 ^b	1055/1098	ring deformation modes
1355 ^b	1318/1326/1366	central C-C stretching modes
1467	1538	CH bend and central CC stretch

^a This feature is wider than the others and likely combines two unresolved vibrational peaks.

^b Several of the modes listed could contribute since they have similar character.

An interesting question in this context is whether the N_2 ligand perturbs the Cu^+ complex significantly. Figure 6 compares the spectra of $[\text{Cu-N}_2]^+$ and Cu^+ at room temperature. The overall structure of the band is rather similar, and the origin of the $\pi\pi^*$ band is at the same energy in both cases. The different relative intensities across the band are due to the fact that the fragment channel for Cu^+ (loss of a neutral Cu atom) is predicted to have a threshold energy of the same order of magnitude as the photon energy (PBE0/def2-TZVP calculations give 4.30 eV for this process, see Table 1). The signal in the lower energy portion is therefore strongly

suppressed due to kinetic shifts. This interpretation is corroborated by the fact that fragment signal from bare Cu^+ was already weak at room temperature and too weak to be registered at cryogenic trap temperatures. The similarity of the $\pi\pi^*$ bands suggests that N_2 is only a spectator, and that the electronic structure of Cu^+ and $[\text{Cu-N}_2]^+$ is largely unperturbed in the region of the $\pi\pi^*$ band. The similarity between Cu^+ and $[\text{Cu-N}_2]^+$ is also evident from the strong similarity of the vibrational progressions (see Supplementary Information, Tables S1 and S2). Both bipy and $[\text{Cu-N}_2]^+$ have a symmetry forbidden excited state below the $\pi\pi^*$ state, and we assume that the excited-state lifetimes are similar.

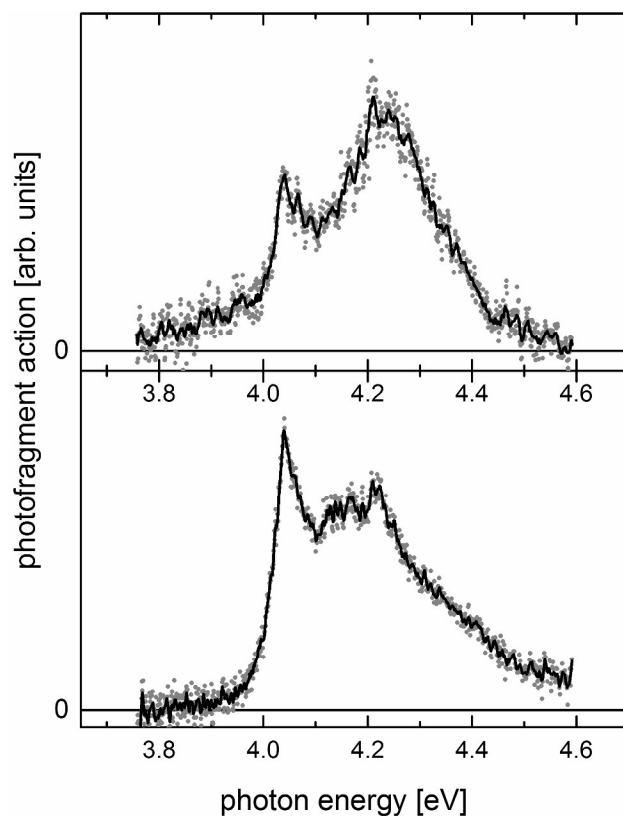


Figure 6. Comparison of the spectra of $[\text{Cu-N}_2]^+$ (loss of N_2 ligand, lower panel) and Cu^+ (loss of neutral Cu, upper panel) at room temperature. The circles show the raw data and the full line represent the same data smoothed by 10-pt-adjacent averaging.

We were not able to probe the $[\text{Cu-N}_2]^+$ complex at lower trap temperatures due to the experimental procedure of forming the complex, but we assume that the residual width of the vibrational features comes from the finite temperature, the excited-state lifetime, or (most likely) from a combination of these two contributions.

III.3. Solvent ligand – H₂O

The UV photodissociation spectrum of $[\text{Cu-OH}_2]^+$ at 50 K trap temperature has sharper features than at room temperature (Figure 7), but is not quite as well resolved as the spectrum for $L = \text{N}_2$. The band contour is similar to that for $L = \text{N}_2$, and the major vibrational features are all found at the same positions from the band origin, which is 0.03 eV higher in energy compared to $L = \text{N}_2$.

For $L = \text{H}_2\text{O}$, there are two states below the bright $\pi\pi^*$ state, one symmetry-forbidden and a weakly allowed transition with metal-to-ligand charge-transfer (MLCT) character (see Table 2 and Figure 8). The latter is likely too weak to be observable in our experiment. The greater width of the spectrum for $L = \text{H}_2\text{O}$ at 50 K compared to $L = \text{N}_2$ at 70 K is interesting, since it runs counter to the intuitive expectation that the spectra should become sharper with decreasing trap temperature, all else being equal. This suggests that the nature of the ligand plays an important role here, not only for the envelope of the spectrum, but also for the lifetime of the excited electronic state. In $[\text{Cu-N}_2]^+$, the ligand is not very perturbative, while in $[\text{Cu-OH}_2]^+$, the presence of an additional state closely below the bright $\pi\pi^*$ state (see Table 2) provides an additional de-excitation pathway, probably shortening the excited-state lifetime relative to that of $[\text{Cu-N}_2]^+$.

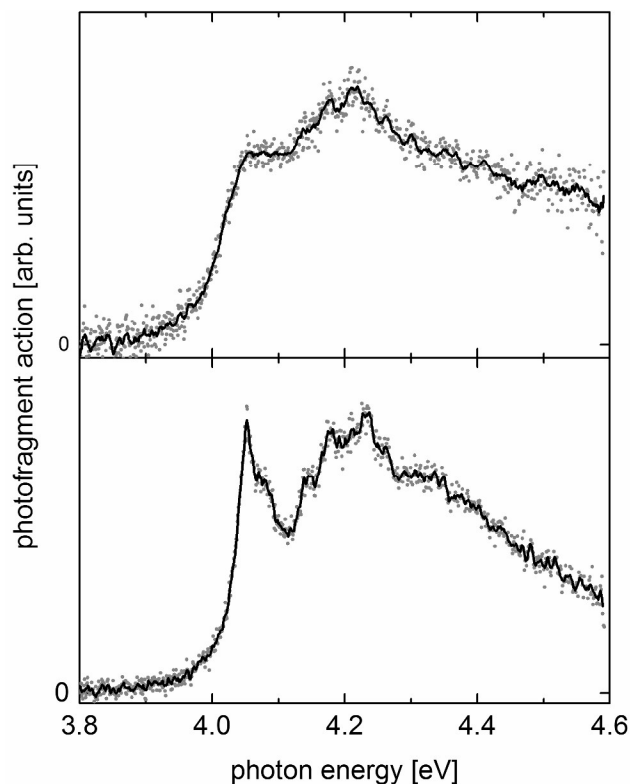


Figure 7. Electronic photodissociation spectrum of $[\text{Cu-OH}_2]^+$ ions (monitoring the loss of water) at room temperature (top) and at 50 K (bottom). The circles show the raw data and the full line represent the same data smoothed by 10-pt-adjacent averaging.

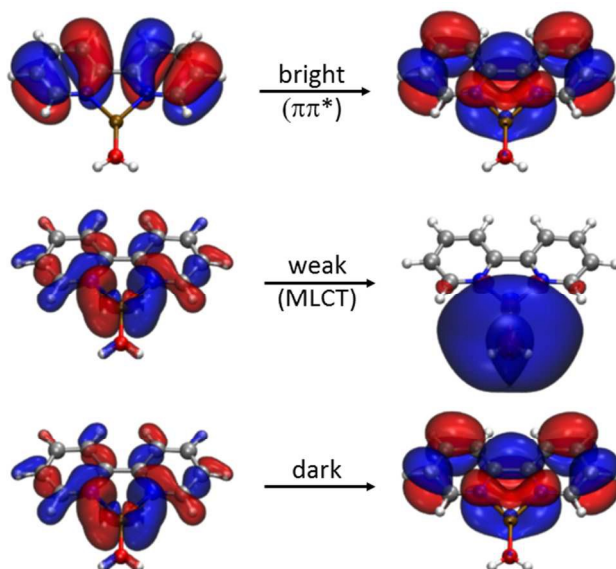


Figure 8. Leading molecular orbitals for the two lowest energy transitions in $[\text{Cu-OH}_2]^+$ (see Table 2 for calculated energies).

III.4. Strongly bound ligand: L = Cl

Figure 9 shows the electronic photodissociation spectrum of $[\text{Cu-Cl}]^+$ ions. These complexes show a pronounced $\pi\pi^*$ band at 4.02 eV, similar to the other $[\text{Cu-L}]^+$ complexes, but they also exhibit a band at ca. 2.7 eV (see Table 2), consistent with a charge-transfer transition. Calculations confirm this assignment, showing ligand-to-ligand Cl-to-bipy charge-transfer (see Figure 10). Note that the calculations show a large difference between the vertical and adiabatic excitation energy for this state (a 0.76 eV difference) due to a significant excited-state relaxation along the Cu-Cl stretching coordinate. The adiabatic energy (2.54 eV) is in reasonably good agreement with the experimental one (2.72 eV).

Both bands have extensive substructure. The structure of the $\pi\pi^*$ band is likely due to vibrational progressions in the excited state, similar to the cases of L = N₂ and H₂O. The origin of the substructure of the charge-transfer band is less clear, particularly since there are several closely lying electronic states calculated to be in the same region (see Table 2). A detailed analysis of the charge-transfer band is not possible at present due to the computational difficulties with this complex. Both the UV and the visible band are rather broad, even at low temperature. The features in the $\pi\pi^*$ band are broader than for the two other ligands in the present study, despite the fact that the Cl ligand has no internal degrees of freedom (in contrast to either N₂ or H₂O) and the trap temperature for the cryogenic spectrum was lower than that for L = N₂. This is again consistent with the assumption that excited-state lifetime is the limiting factor for the width of the observed features, at least for L = H₂O and Cl.

Interestingly, the shape of the charge-transfer band is different at the two temperatures, and the lower energy edge of the band is suppressed at low temperature. This is likely caused by a

kinetic shift at low temperatures, since the threshold energy for the loss of Cl from $[\text{Cu-Cl}]^+$ is calculated to be 2.56 eV, close to the energy of the charge-transfer band.

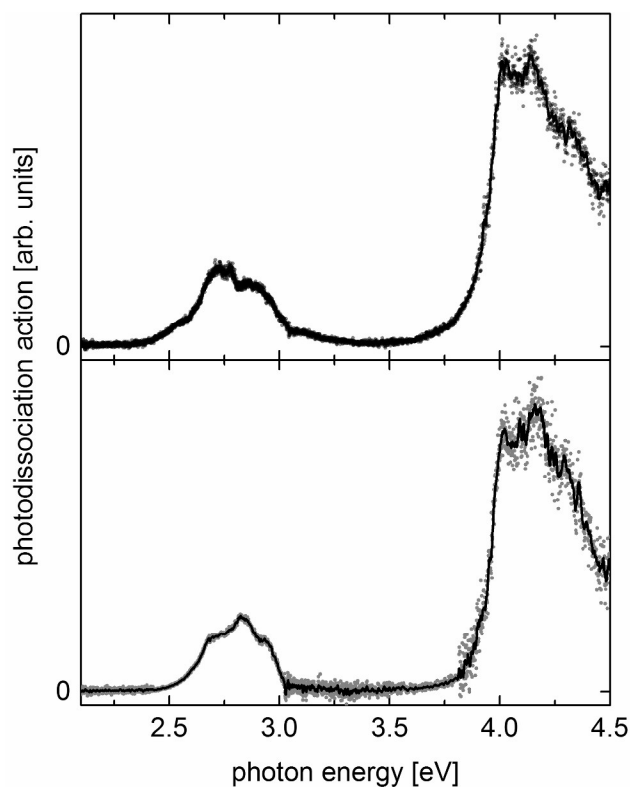


Figure 9. Electronic photodissociation spectrum of $[\text{Cu-Cl}]^+$ ions (monitoring the loss of Cl) at room temperature (top) and at 50 K (bottom). The data points in the photodissociation spectra are the raw data, the full lines are the same data smoothed by 20-pt-adjacent averaging.

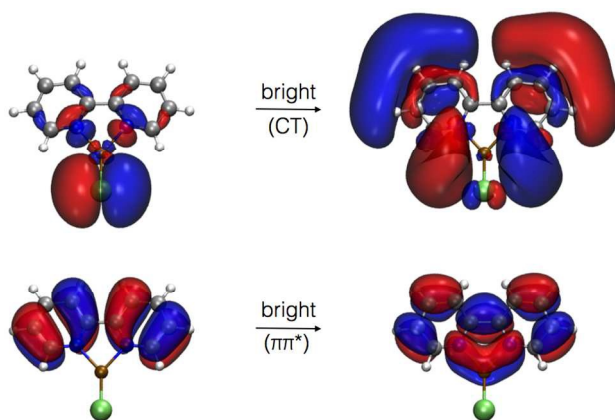


Figure 10. Leading molecular orbitals for the two bright transitions in $[\text{Cu-Cl}]^+$.

IV. Conclusions

We have performed photodissociation spectroscopy and computational analysis of $[\text{Cu-L}]^+$ complexes ($L = \text{N}_2, \text{H}_2\text{O}$ and Cl) in the visible and UV. All three complexes show similar bands in the UV, which are the only observed electronic bands for complexes with N_2 or H_2O ligand. The UV bands are due to the $B_2 \pi\pi^*$ transitions localized on the bipy moiety and show vibrational contours that are consistent primarily with bipy ring deformation modes. Experiments at low temperature show that excited-state lifetime is a determining factor for the width of the vibrational features. The lifetime decreases from N_2 to H_2O to Cl due to an increasing number of lower lying electronic states that offer efficient de-excitation pathways. All complexes have a symmetry forbidden A_2 state closely below the $\pi\pi^*$ state. In the case of $L = \text{H}_2\text{O}$, calculations predict one additional MLCT state, which has too low an oscillator strength to be observed in our experiment. For $L = \text{Cl}$, there is a multitude of lower lying electronic states. At least one of them, characterized as a ligand-to-ligand charge-transfer state, has significant oscillator strength and was observed in the photodissociation spectrum. While the nature of the ligand does not significantly change the position of the bright $\pi\pi^*$ state, it drastically changes the excited-state dynamics.

Acknowledgements

We gratefully acknowledge support of this work by the National Science Foundation under Grant CHE-1361814 (J.M.W.). Instrument development was supported by the NSF Physics Frontier Center at JILA under Grant PHY-1125844. We thank James E. T. Smith for technical assistance. We are indebted to Dr. Michael Z. Kamrath and Prof. Mark A. Johnson for helpful discussion and sharing information during construction and test of our new apparatus. The

computational work was supported by the U.S. National Science Foundation (CHE-1264018, A.I.K.).

References

1. S. M. Barnett, K. I. Goldberg and J. M. Mayer, *Nat. Chem.*, 2012, **4**, 498-502.
2. N. Armaroli, G. Accorsi, F. Cardinali and A. Listorti, in *Photochemistry and Photophysics of Coordination Compounds I*, eds. V. Balzani and S. Campagna, 2007, vol. 280, pp. 69-115.
3. R. D. McAlpine, *J. Mol. Spectrosc.*, 1971, **38**, 441-448.
4. A. Harriman, *J. Photochem.*, 1978, **8**, 205-209.
5. J. Kotlicka and Z. R. Grabowski, *J. Photochem.*, 1979, **11**, 413-418.
6. K. Vinodgopal and W. R. Leenstra, *J. Phys. Chem.*, 1985, **89**, 3824-3828.
7. E. Castellucci, L. Angeloni, G. Marconi, E. Venuti and I. Baraldi, *J. Phys. Chem.*, 1990, **94**, 1740-1745.
8. S. Dhanya and P. K. Bhattacharyya, *J. Photochem. Photobiol. A-Chem.*, 1992, **63**, 179-185.
9. G. Buntinx, R. Naskrecki and O. Poizat, *J. Phys. Chem.*, 1996, **100**, 19380-19388.
10. V. De Waele, G. Buntinx, J. P. Flament and O. Poizat, *Int. J. Quantum Chem.*, 2005, **104**, 794-807.
11. M. W. Blaskie and D. R. McMillin, *Inorg. Chem.*, 1980, **19**, 3519-3522.
12. C. O. Dietrich-Buchecker, P. A. Marnot, J. P. Sauvage, J. R. Kirchhoff and D. R. McMillin, *J. Chem. Soc. Chem. Commun.*, 1983, 513-515.
13. J. R. Kirchhoff, R. E. Gamache, M. W. Blaskie, A. A. Delpaggio, R. K. Lengel and D. R. McMillin, *Inorg. Chem.*, 1983, **22**, 2380-2384.

14. R. A. Rader, D. R. McMillin, M. T. Buckner, T. G. Matthews, D. J. Casadonte, R. K. Lengel, S. B. Whittaker, L. M. Darmon and F. E. Lytle, *J. Am. Chem. Soc.*, 1981, **103**, 5906-5912.
15. J. J. McGarvey, S. E. J. Bell and K. C. Gordon, *Inorg. Chem.*, 1988, **27**, 4003-4006.
16. K. C. Gordon and J. J. McGarvey, *Inorg. Chem.*, 1991, **30**, 2986-2989.
17. S. J. Lind, K. C. Gordon and M. R. Waterland, *J. Raman Spectrosc.*, 2008, **39**, 1556-1567.
18. J. H. Alstrum-Acevedo, M. K. Brennaman and T. J. Meyer, *Inorg. Chem.*, 2005, **44**, 6802-6827.
19. V. Artero and M. Fontecave, *Chem. Soc. Rev.*, 2013, **42**, 2338-2356.
20. P. G. Bomben, B. D. Koivisto and C. P. Berlinguette, *Inorg. Chem.*, 2010, **49**, 4960-4971.
21. Z. F. Chen, J. J. Concepcion, M. K. Brennaman, P. Kang, M. R. Norris, P. G. Hoertz and T. J. Meyer, *Proc. Natl. Acad. Sci. U.S.A.*, 2012, **109**, 15606-15611.
22. J. J. Concepcion, J. W. Jurss, M. K. Brennaman, P. G. Hoertz, A. O. T. Patrocinio, N. Y. M. Iha, J. L. Templeton and T. J. Meyer, *Acc. Chem. Res.*, 2009, **42**, 1954-1965.
23. A. J. Morris, G. J. Meyer and E. Fujita, *Acc. Chem. Res.*, 2009, **42**, 1983-1994.
24. K. J. Young, L. A. Martini, R. L. Milot, R. C. Snoeberger, V. S. Batista, C. A. Schmuttenmaer, R. H. Crabtree and G. W. Brudvig, *Coord. Chem. Rev.*, 2012, **256**, 2503-2520.
25. G. M. Hasselmann and G. J. Meyer, *J. Phys. Chem. B*, 1999, **103**, 7671-7675.
26. L. S. Wang, C. F. Ding, X. B. Wang and S. E. Barlow, *Rev. Sci. Instrum.*, 1999, **70**, 1957-1966.

27. K. R. Asmis, M. Brümmer, C. Kaposta, G. Santambrogio, G. von Helden, G. Meijer, K. Rademann and L. Wöste, *Phys. Chem. Chem. Phys.*, 2002, **4**, 1101-1104.
28. T. R. Rizzo, J. A. Stearns and O. V. Boyarkin, *Int. Rev. Phys. Chem.*, 2009, **28**, 481-515.
29. M. Z. Kamrath, R. A. Relph, T. L. Guasco, C. M. Leavitt and M. A. Johnson, *Int. J. Mass Spectrom.*, 2011, **300**, 91-98.
30. C. Hock, J. B. Kim, M. L. Weichman, T. I. Yacovitch and D. M. Neumark, *J. Chem. Phys.*, 2012, **137**.
31. E. M. Duffy, B. M. Marsh and E. Garand, *J. Phys. Chem. A*, 2015, **119**, 6326-6332.
32. A. B. Wolk, C. M. Leavitt, E. Garand and M. A. Johnson, *Acc. Chem. Res.*, 2014, **47**, 202-210.
33. J. G. Redwine, Z. A. Davis, N. L. Burke, R. A. Oglesbee, S. A. McLuckey and T. S. Zwier, *Int. J. Mass Spectrom.*, 2013, **348**, 9-14.
34. J. C. Marcum, A. Halevi and J. M. Weber, *Phys. Chem. Chem. Phys.*, 2009, **11**, 1740-1751.
35. R. G. Parr and W. Yang, *Density-Functional Theory of Atoms and Molecules*, Oxford University Press, New York, 1989.
36. J. P. Perdew, M. Emzerhof and K. Burke, *J. Chem. Phys.*, 1996, **105**, 9982-9985.
37. F. Weigend and R. Ahlrichs, *Phys. Chem. Chem. Phys.*, 2005, **7**, 3297-3305.
38. R. Ahlrichs, M. Bär, M. Häser, H. Horn and C. Kölmel, *Chem. Phys. Lett.*, 1989, **162**, 165-169.
39. J.-D. Chai and M. Head-Gordon, *Phys. Chem. Chem. Phys.*, 2008, **10**, 6615-6620.
40. A. I. Krylov, *Annu. Rev. Phys. Chem.*, 2008, **59**, 433-462.
41. R. J. Bartlett, *WIREs Comput. Mol. Sci.*, 2012, **2**, 126-138.

42. P. G. Szalay and J. Gauss, *J. Chem. Phys.*, 2000, **112**, 4027-4036.
43. A. I. Krylov, *Accounts Chem. Res.*, 2006, **39**, 83-91.
44. A. I. Krylov, *Chem. Phys. Lett.*, 2001, **338**, 375-384.
45. L. Koziol, S. V. Levchenko and A. I. Krylov, *J. Phys. Chem. A*, 2006, **110**, 2746-2758.
46. E. Epifanovsky, D. Zuev, X. Feng, K. Khistyayev, Y. Shao and A. I. Krylov, *J. Chem. Phys.*, 2013, **139**.
47. Y. Shao, Z. Gan, E. Epifanovsky, A. T. B. Gilbert, M. Wormit, J. Kussmann, A. W. Lange, A. Behn, J. Deng, X. Feng, D. Ghosh, M. Goldey, P. R. Horn, L. D. Jacobson, I. Kaliman, R. Z. Khaliullin, T. Kus, A. Landau, J. Liu, E. I. Proynov, Y. M. Rhee, R. M. Richard, M. A. Rohrdanz, R. P. Steele, E. J. Sundstrom, H. L. Woodcock, III, P. M. Zimmerman, D. Zuev, B. Albrecht, E. Alguire, B. Austin, G. J. O. Beran, Y. A. Bernard, E. Berquist, K. Brandhorst, K. B. Bravaya, S. T. Brown, D. Casanova, C.-M. Chang, Y. Chen, S. H. Chien, K. D. Closser, D. L. Crittenden, M. Diedenhofen, R. A. DiStasio, Jr., H. Do, A. D. Dutoi, R. G. Edgar, S. Fatehi, L. Fusti-Molnar, A. Ghysels, A. Golubeva-Zadorozhnaya, J. Gomes, M. W. D. Hanson-Heine, P. H. P. Harbach, A. W. Hauser, E. G. Hohenstein, Z. C. Holden, T.-C. Jagau, H. Ji, B. Kaduk, K. Khistyayev, J. Kim, J. Kim, R. A. King, P. Klunzinger, D. Kosenkov, T. Kowalczyk, C. M. Krauter, K. U. Lao, A. D. Laurent, K. V. Lawler, S. V. Levchenko, C. Y. Lin, F. Liu, E. Livshits, R. C. Lochan, A. Luenser, P. Manohar, S. F. Manzer, S.-P. Mao, N. Mardirossian, A. V. Marenich, S. A. Maurer, N. J. Mayhall, E. Neuscamman, C. M. Oana, R. Olivares-Amaya, D. P. O'Neill, J. A. Parkhill, T. M. Perrine, R. Peverati, A. Prociuk, D. R. Rehn, E. Rosta, N. J. Russ, S. M. Sharada, S. Sharma, D. W. Small, A. Sodt, T. Stein, D. Stueck, Y.-C. Su, A. J. W. Thom, T. Tsuchimochi, V. Vanovschi, L. Vogt, O. Vydrov, T. Wang, M. A. Watson, J.

- Wenzel, A. White, C. F. Williams, J. Yang, S. Yeganeh, S. R. Yost, Z.-Q. You, I. Y. Zhang, X. Zhang, Y. Zhao, B. R. Brooks, G. K. L. Chan, D. M. Chipman, C. J. Cramer, W. A. Goddard, III, M. S. Gordon, W. J. Hehre, A. Klamt, H. F. Schaefer, III, M. W. Schmidt, C. D. Sherrill, D. G. Truhlar, A. Warshel, X. Xu, A. Aspuru-Guzik, R. Baer, A. T. Bell, N. A. Besley, J.-D. Chai, A. Dreuw, B. D. Dunietz, T. R. Furlani, S. R. Gwaltney, C.-P. Hsu, Y. Jung, J. Kong, D. S. Lambrecht, W. Liang, C. Ochsenfeld, V. A. Rassolov, L. V. Slipchenko, J. E. Subotnik, T. Van Voorhis, J. M. Herbert, A. I. Krylov, P. M. W. Gill and M. Head-Gordon, *Mol. Phys.*, 2015, **113**, 184-215.
48. A. I. Krylov and P. M. W. Gill, *WIREs Comput. Mol. Sci.*, 2013, **3**, 317-326.
49. R. Baer and D. Neuhauser, *Phys. Rev. Lett.*, 2005, **94**.
50. E. Livshits and R. Baer, *Phys. Chem. Chem. Phys.*, 2007, **9**, 2932-2941.
51. J. Fine, K. Diri, A. I. Krylov, C. Nemirow, Z. Lu and C. Wittig, *Mol. Phys.*, 2012, **110**, 1849-1862.
52. C. L. Janssen and I. M. B. Nielsen, *Chem. Phys. Lett.*, 1998, **290**, 423-430.
53. T.-C. Jagau, D. B. Dao, N. S. Holtgrewe, A. I. Krylov and R. Mabbs, *J. Phys. Chem. Lett.*, 2015, **6**, 2786-2793.